


 Cite this: *Chem. Commun.*, 2025, 61, 366

 Received 29th September 2024,  
Accepted 19th November 2024

DOI: 10.1039/d4cc05095a

rsc.li/chemcomm

# Bifunctional chlorhexidine-based covalent organic polymers for CO<sub>2</sub> capture and conversion without a co-catalyst†

 Ruiying Zhang,<sup>ab</sup> Yue Shen,<sup>b</sup> Lin Liu<sup>ib</sup>\*<sup>a</sup> and Zhengbo Han<sup>ib</sup>\*<sup>a</sup>

**Two new cobalt/zinc-coordinated bifunctional covalent organic polymers (COP-Co and COP-Zn) based on chlorhexidine are prepared as heterogeneous catalysts for carbon dioxide (CO<sub>2</sub>) conversion. Due to the Cl<sup>-</sup> nucleophile and cobalt/zinc Lewis acid sites, COP-Co and COP-Zn can efficiently convert CO<sub>2</sub> and epoxides into cyclic carbonates under mild conditions without a co-catalyst.**

Carbon dioxide (CO<sub>2</sub>) is accumulating in the atmosphere, causing many global greenhouse effect problems; hence, slowing the current trend of global warming needs to be addressed.<sup>1</sup> Mounting attention has been given to converting CO<sub>2</sub> into high value-added products.<sup>2</sup> Among diverse CO<sub>2</sub> conversion technologies, the cyclic carbonates formed by cycloaddition of CO<sub>2</sub> with epoxides are high-value fine chemical intermediates and are indispensable for both the pharmaceutical and organic synthesis industries.<sup>3</sup> Traditional homogeneous catalysts such as halogen ionic liquids and metal complexes have played a dominant role in this reaction.<sup>4</sup> However, these homogeneous catalysts are faced with difficulties in the recovery of the catalyst and purification of the product, thus increasing the cost.<sup>5</sup> In contrast, heterogeneous catalysts with structural and thermal stability are beneficial for recyclability.<sup>6</sup> Nevertheless, harsh reaction conditions such as high pressure and temperature obstruct factory needs in large-scale production. Hence, considerable efforts have been made to search for suitable catalysts for CO<sub>2</sub> conversion.

Porous materials such as metal-organic frameworks and covalent organic frameworks have been extensively developed as typical heterogeneous catalysts for CO<sub>2</sub> conversion owing to their large surface area, high porosities, and good stability.<sup>7</sup> Among them, covalent organic polymers (COPs) have emerged

as promising candidates for applications owing to their high porosity, fast kinetics, and designable pore structure.<sup>8</sup> Several metal ions such as Zn, Co, Al, and Cu have been introduced into COP networks to provide a wide variety of metal-functionalized COPs.<sup>6,9</sup> Due to the porous structures and the Lewis acid sites of the incorporated metal moieties, the adsorption capacity and the catalytic performance of these COPs can be significantly enhanced. For example, Deng *et al.* reported a Zn-based COP catalyst for efficient CO<sub>2</sub> cycloaddition.<sup>10</sup> Chen *et al.* developed a series of aluminum porphyrin-based COPs, which are considered excellent catalysts for converting CO<sub>2</sub> into cyclic carbonates.<sup>11</sup> Consequently, great success encouraged researchers to seek COP materials for CO<sub>2</sub> capture and applications.

Chlorhexidine (CHX) with abundant neutral tetradentate donors and chlorines in the skeleton exhibits excellent coordination ability for many metal ions. Moreover, Cl<sup>-</sup> is regarded as the nucleophile in catalytic reactions. Generally, the exploration of chlorhexidine has focused on clinical antimicrobial research but has rarely been used in the synthesis of COPs. For instance, three new chlorhexidine complexes synthesized from copper chloride, copper bromide, and acetate indicate that chlorhexidine and copper salt has a quadrilateral twisted octahedral symmetry with a ratio of 1 : 1.<sup>12</sup> Therefore, chlorhexidine has been identified as a prospective candidate for developing COP catalysts.

Herein, two new metal-functionalized COPs (COP-Co and COP-Zn) are synthesized using CHX-Co/Zn complexes (CHX = chlorhexidine) and nitrogen-rich tri(1*H*-imidazole-1-yl)-1,3,5-triazine (TIT) under solvothermal conditions (Fig. 1). Due to the synergistic effects of Co/Zn Lewis acid sites and Cl<sup>-</sup> nucleophile, the COP-Co and COP-Zn catalysts can capture and convert CO<sub>2</sub> under mild conditions in the absence of a co-catalyst.

The morphological structures of COP-Co and COP-Zn were analyzed by scanning electron microscopy (SEM) and transmission electron microscopy (TEM). Fig. 2a and b show that COP-Co is composed of relatively uniform nanoparticles with a size of 200 nm and possess a porous structure, which can facilitate epoxide penetration and fast reaction kinetics. The element mappings of COP-Co further show that C, N, Cl, and Co

<sup>a</sup> College of Chemistry, Liaoning University, Shenyang 110036, P. R. China.  
E-mail: ceshzb@lnu.edu.cn, liulin@lnu.edu.cn

<sup>b</sup> College of Science, Northeastern University, Shenyang 110819, Liaoning, P. R. China

† Electronic supplementary information (ESI) available. See DOI: <https://doi.org/10.1039/d4cc05095a>

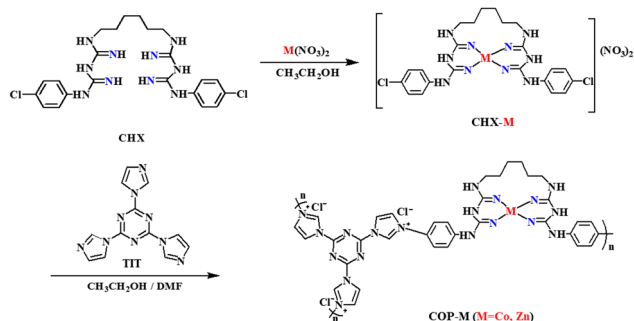


Fig. 1 Synthesis route of COP-M (M = Co, Zn).

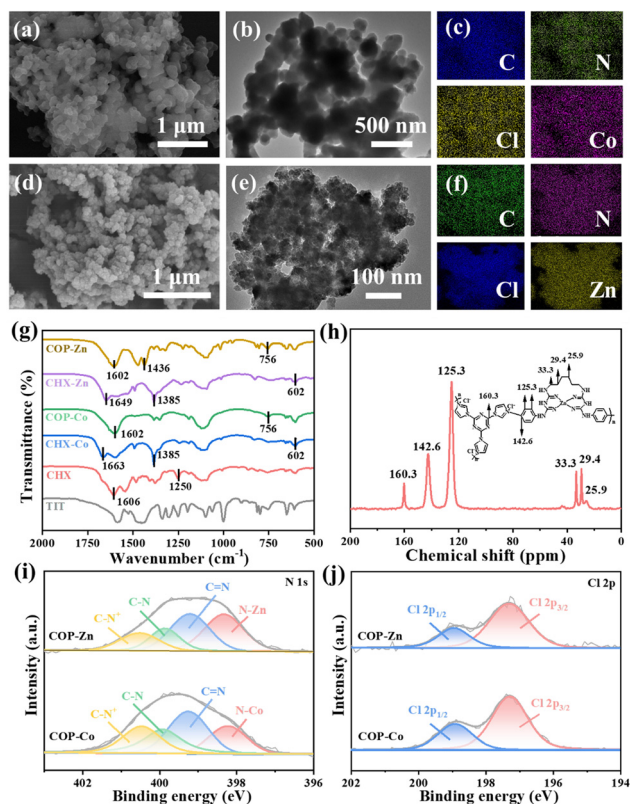


Fig. 2 (a) SEM image, (b) TEM image, and (c) element mappings of COP-Co. (d) SEM image, (e) TEM image, and (f) element mappings of COP-Zn. (g) FT-IR spectra of TIT, CHX, CHX-Co, COP-Co, CHX-Zn, and COP-Zn. (h) Solid-state  $^{13}\text{C}$ -NMR spectrum of COP-Zn. (i) High-resolution N 1s and (j) Cl 2p XPS spectra of COP-Zn and COP-Co.

elements are uniformly distributed in the skeleton (Fig. 2c and Fig. S1, ESI $^\dagger$ ). Fig. 2d shows that COP-Zn consists of densely packed nanoparticles. The TEM image of COP-Zn demonstrates a remarkably aggregated nanoparticle structure (Fig. 2e). Additionally, the elemental mappings of COP-Zn illustrate the homogeneous distribution of C, N, Cl, and Zn elements in the COP-Zn framework (Fig. 2f and Fig. S2, ESI $^\dagger$ ).

The broad peaks were observed in X-ray diffraction patterns, proving the amorphous states of COP-Co and COP-Zn (Fig. S3, ESI $^\dagger$ ). This is caused by the disordered accumulation of polymers during the formation process. The Fourier transform

infrared (FTIR) spectra were carried out to certify the structures of COP-Co and COP-Zn (Fig. 2g). The peak at  $602\text{ cm}^{-1}$  of CHX-Co and CHX-Zn related to the formation of Co/Zn–N bonds. The vibration peak at  $1250\text{ cm}^{-1}$  belonging to C–Cl groups of CHX disappears, confirming the formation of COP-Co and COP-Zn. Furthermore, the molecular structure of COP-Zn was further illustrated by the solid-phase  $^{13}\text{C}$ -NMR spectra (Fig. 2h). The peak at 160.3 ppm is assigned to the triazine ring carbon. The peak at 33.3 ppm is derived from C–N groups, while the other two lower intensity peaks at 25.9 and 29.4 ppm are ascribed to sp-hybridized –CH carbons in the CHX moiety. The peak at 142.6 ppm corresponded to the aromatic ring carbon shifts to 125.3 ppm in COP-Zn, indicating that CHX-Zn is connected to imidazole to produce imidazolium.<sup>13</sup> The molecular weight and polydispersity index of COP-Co tested by gel permeation chromatography are  $18\,841\text{ g mol}^{-1}$  and 2.05, respectively.

The chemical compositions of the samples were examined by X-ray photoelectron spectra (XPS) tests with Ar ion etching 50 nm deep. The atomic compositions of Co and Zn are determined to be 7.0 wt% and 7.5 wt%, respectively. Several peaks of COP-Zn located at around 202, 285, 400, and 1035 eV can be ascribed to Cl 2p, C 1s, N 1s, and Zn 2p, respectively (Fig. S4, ESI $^\dagger$ ). The peaks of COP-Co located at 202, 285, 100, and 800 eV belong to Cl 2p, C 1s, N 1s, and Co 2p, respectively (Fig. S5, ESI $^\dagger$ ). The C 1s spectra of COP-Co and COP-Zn exhibit three peaks at 288.9, 286.3, and 284.8 eV, which are ascribed to C=N, C–N, and C=C/C–C groups, respectively (Fig. S6, ESI $^\dagger$ ).<sup>14</sup> The N 1s spectra of COP-Co and COP-Zn are decomposed into four peaks: 400.5, 399.9, 399.2, and 398.2 eV, which are related to C–N $^+$ , C–N, C=N, and N–Co/Zn units, respectively (Fig. 2i).<sup>15</sup> Additionally, the N 1s spectra of CHX, CHX-Co, and CHX-Zn are explored. In contrast with CHX, the peaks that appeared at around 455.6 eV belong to N–Zn and N–Co metal bonds, indicating the formation of CHX-Co/Zn (Fig. S7, ESI $^\dagger$ ). The Cl 2p peaks of COP-Co and COP-Zn that appeared at 198.9 eV and 197.3 eV are ascribed to chloride Cl $^-$ , relating to the formation of COP-Co and COP-Zn (Fig. 2j). Compared to COP-Co and COP-Zn, the Cl 2p peaks of CHX, CHX-Co, and CHX-Zn located at 200.3 eV and 201.9 eV correspond to organic Cl (Fig. S8, ESI $^\dagger$ ). This result proves that CHX-Co/Zn is associated with TIT and the organic Cl is converted into a chloride Cl $^-$ .<sup>16</sup> The peaks of Zn 2p located at 1023 eV and 1046 eV correspond to Zn 2p $_{3/2}$  and Zn 2p $_{1/2}$ , respectively (Fig. S9, ESI $^\dagger$ ). The peaks of the Co 2p spectra appearing at 784 eV and 801 eV are associated with Co 2p $_{3/2}$  and Co 2p $_{1/2}$ , respectively. Both peaks are accompanied by satellite peaks at 789 eV and 805 eV (Fig. S10, ESI $^\dagger$ ). The thermogravimetric analysis results indicate that COP-Co and COP-Zn could be stable up to 210 °C and 222 °C, respectively, indicating their good thermal stability. The glass transition points of COP-Co detected by differential scanning calorimeter are 155 °C (Fig. S11, ESI $^\dagger$ ).

The surface areas and the porous structures of COP-Co and COP-Zn were investigated by N $_2$  and CO $_2$  adsorption/desorption tests. The Brunauer–Emmett–Teller (BET) surface area of COP-Co is  $136\text{ m}^2\text{ g}^{-1}$ . COP-Co exhibits both type-I and type-IV

behaviors, indicating that COP-Co is composed of micropores and mesopores (Fig. S12, ESI†).<sup>12</sup> The pore size of COP-Co characterized using non-local density functional theory is 0.7 and 3.8 nm. Due to the degradation and agglomeration of the frameworks, the COP-Zn exhibits a type-IV curve with an H<sub>3</sub>-type hysteresis ring and a much lower BET surface area (47 m<sup>2</sup> g<sup>-1</sup>) than COP-Co. The median pore size of COP-Zn calculated by the Barrett-Joyner-Halenda method is in the range of 2.6–3.5 nm (Fig. S13, ESI†). The chemical adsorption abilities of CO<sub>2</sub> and the possible reaction mechanisms of COP-Co/COP-Zn are characterized by the Langmuir model based on eqn (S1) (ESI†) (Fig. S14, ESI†).<sup>14</sup> The Langmuir surface areas of COP-Co and COP-Zn are 211 m<sup>2</sup> g<sup>-1</sup> and 79 m<sup>2</sup> g<sup>-1</sup>, respectively. At 273 K, COP-Co and COP-Zn display CO<sub>2</sub> adsorption capacity of 57.3 mg g<sup>-1</sup> and 27.6 mg g<sup>-1</sup>, respectively. At 298 K, the CO<sub>2</sub> adsorption capacities of COP-Co and COP-Zn are 31.2 mg g<sup>-1</sup> and 22.5 mg g<sup>-1</sup> (Table S1, ESI†). These results verify that CO<sub>2</sub> capture could be based on chemical absorption. The strong CO<sub>2</sub> capture abilities are attributed to the large surface area.

Based on the above results, the attractive structures and high CO<sub>2</sub> adsorption capacities endow COP-Co and COP-Zn as potential catalysts for the cycloaddition of CO<sub>2</sub> and epoxides to form cyclic carbonates. The reactions were purged to 1.0 MPa pressure under co-catalyst-free conditions. The products were obtained by removing the COP-Co and COP-Zn from the reaction system through centrifugation. The conversion was determined by eqn (S2) (ESI†) and gas chromatography (Fig. S15, ESI†). To investigate the systematic optimization of reaction parameters such as reaction temperature, catalyst amount, and reaction time, typical reactions were conducted using propylene oxide (PO) substrate and CO<sub>2</sub>. When the weight of COP-Co was 30 mg, 40 mg, 50 mg, and 60 mg, the PO conversions were 17.3%, 40.8%, 46.3%, and 46.8%, respectively (Table 1, entries 1–4). The conversion increases according to the amount of COP-Co; that is, the concentration of the catalytic active site determines the catalytic efficiency. When the temperature increases from 80 °C to 90 °C, the conversion of PO advances from 46.8% to 49% (Table 1, entry 5). However, when the reaction temperature rises from 90 °C to 100 °C, the conversion increases almost negligibly (Table 1, entry 6). These results verify that 90 °C is the optimal temperature. When the reaction times are 3, 6, 9, and 12 hours, the conversions are 50.7%, 59%, 80.2%, and 98.4%, respectively (Table 1, entries 6–9). Observably, the optimized reaction conditions (50 mg catalyst, 90 °C, 12 hours, 1 MPa) are obtained and applied to the subsequent catalytic reactions. Moreover, the epoxides with different sizes were investigated under the optimized conditions (Table 1, entries 9–18). All of the substrates are effectively converted into their corresponding cyclic carbonates. When COP-Co is used as a catalyst, the conversion of PO is 98.4% with a turnover number (TON) value of 164 while the COP-Zn catalyst represents a conversion of 90.2% with a TON value of 150. Compared with the reported catalysts, COP-Co and COP-Zn show good catalytic performance for CO<sub>2</sub> cycloaddition under co-catalyst-free conditions (Table S2, ESI†). Both COP-Co and COP-Zn catalysts exhibit a certain size selection effect. With the

**Table 1** Cycloaddition of CO<sub>2</sub> and different epoxides catalyzed by COP-Co and COP-Zn in the absence of a co-catalyst

Entry	R	Amount (mg)	Time (h)	Conversion <sup>a</sup> (%)	TON <sup>b</sup>
1 <sup>ee</sup>	Me	30	3	17.3	24
2 <sup>ee</sup>	Me	40	3	40.8	85
3 <sup>ee</sup>	Me	50	3	46.3	77
4 <sup>ee</sup>	Me	60	3	46.8	65
5 <sup>ee</sup>	Me	50	3	49.0	82
6 <sup>gg</sup>	Me	50	3	50.7	85
7 <sup>ef</sup>	Me	50	6	59.0	98
8 <sup>ef</sup>	Me	50	9	80.2	131
9 <sup>ef</sup>	Me	50	12	98.4	164
10 <sup>df</sup>	Me	50	12	90.2	150
11 <sup>ef</sup>	CH <sub>2</sub> Cl	50	12	93.1	155
12 <sup>df</sup>	CH <sub>2</sub> Cl	50	12	87.7	146
13 <sup>ef</sup>	Et	50	12	83.0	138
14 <sup>df</sup>	Et	50	12	55.4	92
15 <sup>ef</sup>	Ph	50	12	53.1	89
16 <sup>df</sup>	Ph	50	12	20.6	34
17 <sup>ef</sup>	C <sub>4</sub> H <sub>9</sub> OCH <sub>2</sub>	50	12	40.0	67
18 <sup>df</sup>	C <sub>4</sub> H <sub>9</sub> OCH <sub>2</sub>	50	12	16.9	28

<sup>a</sup> Conversions were determined by gas chromatography. <sup>b</sup> TON = (mole of products)/(mole of active sites). Reaction conditions: epoxides (10 mmol), CO<sub>2</sub> (1 MPa). Catalyst. <sup>c</sup> COP-Co. <sup>d</sup> COP-Zn. Temperature. <sup>e</sup> 80 °C. <sup>f</sup> 90 °C. <sup>g</sup> 100 °C.

substrate molecular size increasing, the conversions of epoxides obviously decrease.<sup>17</sup>

For heterogeneous catalysts, the recyclability is an important factor to evaluate catalytic performance. To probe the recyclability of COP-Co and COP-Zn, cycling reactions were performed using PO as the substrate under optimized conditions. The COP-Co and COP-Zn catalysts were recovered and reused by centrifugation, washing, and drying for multiple cycles (Fig. S16, ESI†). The conversion of the COP-Co catalyst decreases slightly from 98.4% to 85.1% after 5 cycles at a relatively mild CO<sub>2</sub> pressure (1 MPa) and temperature (90 °C), demonstrating the recyclability and stability of COP-Co. Unfortunately, the cycling stability of COP-Zn is relatively poor. After five cycles of COP-Zn, the PO conversion decreases from 90.2% to 80.5%. This is due to the fact that trace amounts of water in the catalytic reaction system form inactive zinc species, resulting in the destruction of the reactivity.<sup>18</sup> After five cycles, the morphology of the COP-Co and COP-Zn catalysts remains nearly unchanged, illustrating the remarkable structural stability (Fig. S17, ESI†). Leaching tests were carried out to verify the heterogeneous properties of the COP-Co and COP-Zn catalysts. When the catalysts are removed from the reaction systems, the increase of conversion is negligible, proving that COP-Co and COP-Zn are heterogeneous catalysts (Fig. S18, ESI†).

Based on the current research results,<sup>19</sup> the possible reaction mechanism of COP-Co for the cycloaddition reaction of CO<sub>2</sub> with epoxides is proposed (Fig. 3). Firstly, oxygen atoms in

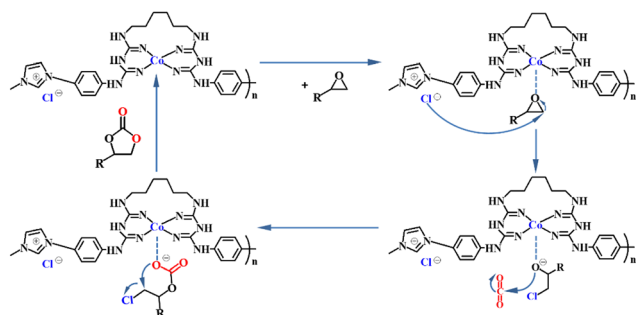


Fig. 3 Proposed catalysis process of COP-Co for CO<sub>2</sub> conversion.

the epoxides are coordinated to metal Lewis acid sites (Co<sup>2+</sup> for COP-Co) to form a powerful electron-rich intermediate that can activate the epoxide ring. Meanwhile, Cl<sup>-</sup> ions attack the C–O bond with less steric hindrance in epoxides, leading to the ring-opening reaction. Then, the CO<sub>2</sub> enriched in the COP-Co and COP-Zn catalysts interacts with the ring-opening epoxides to generate alkoxy anions.<sup>20</sup> Furthermore, the N-rich framework of COP-Co can increase the adsorption of CO<sub>2</sub>, thus improving the CO<sub>2</sub> capture ability and accelerating the reaction. Finally, the alkoxy anion closes its ring to form cyclic carbonate and COP-Co is regenerated.

In conclusion, two new bifunctional cationic COP-Co and COP-Zn based on CHX are prepared as the heterogeneous catalysts for CO<sub>2</sub> conversion. Both COP-Co and COP-Zn present high BET surface area and good CO<sub>2</sub> adsorption capacity. The COP-Co and COP-Zn exhibit certain size selection effects as heterogeneous catalysts for CO<sub>2</sub> cycloaddition reaction. The Cl<sup>-</sup> acts as a nucleophile to facilitate the ring-opening of epoxides and cobalt/zinc act as Lewis acid centers. Due to the synergistic effects, the COP-Co and COP-Zn can efficiently convert CO<sub>2</sub> and epoxides into cyclic carbonates with high conversion, durability, and recyclability under relatively mild conditions in the absence of a co-catalyst. This work expands the categories of COPs for future applications and provides a new way to capture and transform CO<sub>2</sub>. Meanwhile, due to the limitations of open-air implementation, these COPs for CO<sub>2</sub> capture from laboratory to industrial applications still require in-depth exploration.

The authors kindly acknowledge financial support from the National Natural Science Foundation of China (22171121), Applied Basic Research Plan of Liaoning Province (2023JH2/101300007), the Chey Institute for Advanced Studies' International Scholar Exchange Fellowship for the academic year of 2023–2024, and the Fundamental Research Funds for Public Universities in Liaoning.

## Data availability

The data supporting this article have been included as part of the ESI.†

## Conflicts of interest

There are no conflicts to declare.

## Notes and references

- S. Yu, H. Yamauchi, S. Wang, A. Aggarwal, J. Kim, K. Gordiz, B. T. Huang, H. B. Xu, D. J. Zheng, X. Wang, H. Iriawan, D. Menga and Y. Shao-Horn, *Nat. Catal.*, 2024, 3037.
- Q. W. Song, Z. H. Zhou and L. N. He, *Green Chem.*, 2017, **19**, 3707–3728; E. J. Beckman, *Nature*, 2016, **531**, 180–181.
- L. Wang, G. Zhang, K. Kodama and T. Hirose, *Green Chem.*, 2016, **18**, 1229–1233; Z. H. Wang, Y. C. Li, Z. H. Ma, D. Z. Wang and X. D. Ren, *Iscience*, 2024, **27**, 110437.
- S. J. Zeng, X. Zhang, L. P. Bai, X. C. Zhang, H. Wang, J. J. Wang, D. Bao, M. D. Li, X. Y. Liu and S. J. Zhang, *Chem. Rev.*, 2017, **117**, 9625–9673.
- M. Lin, Q. Cai, Z. Xiao, H. Chen, B. Wang, C. W. Qiu, J. N. Shen, J. L. Long, W. X. Dai, S. T. Han, X. X. Wang, Z. Z. Zhang and H. L. Xi, *Inorg. Chem.*, 2024, **63**, 14591–14601.
- R. Abazari, N. Ghorbani, J. Shariati, R. S. Varma and J. J. Qian, *Inorg. Chem.*, 2024, **63**, 12667–12680.
- P. X. Guan, J. K. Qiu, Y. L. Zhao, H. Y. Wang, Z. Y. Li, Y. L. Shi and J. J. Wang, *Chem. Commun.*, 2019, **55**, 12459–12462.
- J. Guo, C. Lin, Z. Xia and Z. Xiang, *Angew. Chem., Int. Ed.*, 2018, **57**, 12567–12572.
- J. Zheng, M. Wahiduzzaman, D. Barpaga, B. A. Trumpf, O. Y. Gutierrez, P. Thallapally, S. Ma, B. P. McGrail, G. Maurin and R. K. Motkuri, *Angew. Chem., Int. Ed.*, 2021, **60**, 18037–18043; B. Y. Wang, X. Y. Cao, L. X. Wang, X. Y. Meng, Y. Wang and W. Sun, *Inorg. Chem.*, 2024, **63**, 9156–9163.
- W. Zhou, Q.-W. Deng, G.-Q. Ren, L. Sun, L. Yang, Y.-M. Li, D. Zhai, Y.-H. Zhou and W.-Q. Deng, *Nat. Commun.*, 2020, **11**, 4481.
- M. Chen, X. Liu, Y. Yang, W. Xu, K. Chen and R. Luo, *ACS Appl. Mater. Interfaces*, 2023, **15**, 8263–8274.
- M. Badea, R. Olar, M. Ilis, R. Georgescu and M. Calinescu, *J. Therm. Anal. Calorim.*, 2013, **111**, 1763–1770.
- R. Zhang, D. Du, Y. Wang, T. A. Otitoju, Z. Feng and T. Sun, *Energy Storage Mater.*, 2024, **65**, 103164.
- F. Raganati, M. Alfe, V. Gargiulo, R. Chirone and P. Ammendola, *Chem. Eng. Res. Des.*, 2018, **134**, 540–552; H. J. Esfahani, A. Ghaemi and S. Shahhosseini, *Sci. Rep.*, 2024, **14**, 18871.
- R. Zhang, Y. Tian, T. Otitoju, Z. Feng, Y. Wang and T. Sun, *Small*, 2023, **19**, 2302148.
- D. Luo, Z.-Y. Zhang, H. Yuan, X.-Y. Yu, X. Gao, Z. Hu and C.-R. Chang, *Chem. Eng. J.*, 2024, **481**, 148129; Y. Liu, J. Li, Z. Zhang, Y. Hou, L. Wang and J. Zhang, *Inorg. Chem.*, 2022, **61**, 17438–17447.
- X. F. Zhang, H. T. Liu, P. F. An, Y. N. Shi, J. Y. Han, Z. J. Yang, C. Long, J. Guo, S. L. Zhao, K. Zhao, H. J. Yin, L. R. Zheng, B. H. Zhang, X. P. Liu, L. J. Zhang, G. D. Li and Z. Y. Tang, *Sci. Adv.*, 2020, **6**, eaaz4824.
- Y. Xu, P. Wang, X. J. Zhan, W. L. Dai, Q. Li, J. P. Zou and X. B. Luo, *J. Colloid Interface Sci.*, 2024, **673**, 134–142.
- T.-T. Liu, J. Liang, Y.-B. Huang and R. Cao, *Chem. Commun.*, 2016, **52**, 13288–13291.
- Y. Chen, F. F. Li, L. Y. Liu and Y. H. Zhou, *Chem. Eng. J.*, 2024, **490**, 151657; Y. F. Wang, H. M. Liu, Q. J. Shi, Z. R. Miao, H. H. Duan, Y. Wang, H. P. Rong and J. T. Zhang, *Angew. Chem., Int. Ed.*, 2024, **63**, e202404911.